PHOTON STRUCTURE FUNCTIONS AT LEP

K.K.G. Freudenreich

Labor für Hochenergiephysik, Institut für Teilchenphysik, ETH Zürich, Switzerland;
e-mail: Klaus.Freudenreich@cern.ch

The hadronic and leptonic photon structure functions at LEP are reviewed and compared to previous experiments.

1 Introduction

The study of the scattering of a virtual photon on a quasi real one has been extended quite considerably at LEP both in statistics and in kinematic range.

The two-photon process is depicted in Fig. 1 where the kinematic variables used are indicated as well. One distinguishes three types of two-photon events: i) Both final state electrons remain undetected, ii) one electron is detected (single-tag) and iii) both electrons are detected (double tag events). The presently available statistics of double tag events is about two orders of magnitude lower than that of the single-tag ones. In the following we shall only consider single-tag events, where at the same time an anti-tag condition is imposed on the second electron.

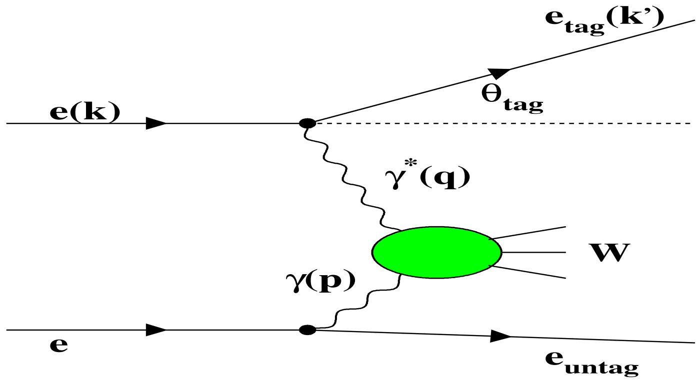

Figure 1: Feynman diagram of the two-photon process defining the kinematical variables.

The kinematical variables are defined, as usual, in the following. Q^2 is the four-momentum transfer squared of the probe photon at the tagged electron vertex:
$Q^2 = -q^2 = -(k-k')^2 = 2 \cdot E_{beam} E_{tag} (1 - cos\Theta_{tag})$
$P^2 = -p^2$ is the four-momentum transfer squared of the target photon. The target photons are typically collinear with the beams - the maximum lab angle of the untagged electron is the minimum lab angle of the tagged electron. In single-tag events the target photon is, therefore, quasi real. The center of mass squared of the $\gamma\gamma$ system is given by:
$W^2 = (q+p)^2 = (\sum_i E_i)^2 - (\sum_i \overrightarrow{p_i})^2$
where i runs over the produced particles, either hadrons or leptons. The Bjorken x can then be derived as:
$x = \frac{-q^2}{2p\cdot q} = \frac{Q^2}{Q^2+P^2+W^2} \approx \frac{Q^2}{Q^2+W^2}$

The inelasticity y is, finally, given by:

$$y = \frac{p\cdot q}{p\cdot k} = 1 - \frac{E_{tag}}{E_{beam}} cos^2(\frac{\theta_{tag}}{2}) \ << \ 1$$

The differential cross-section for the two-photon process $e^+e^- \to e^+e^-$ + X contains two "structure functions":
$\frac{d^2\sigma}{dxdQ^2} = \frac{2\pi\alpha^2}{xQ^4}[(1+(1-y)^2)F_2^\gamma(x,Q^2) - y^2 F_L^\gamma(x,Q^2)]$

$F_2^\gamma(x,Q^2)$ depends on the parton densities of both "transverse" and "longitudinal" photons. $F_L^\gamma(x,Q^2)$ is for "longitudinal" photons only. Since the tag angle θ_{tag} is very small and the tag energy close to the beam energy, the factor y^2 which multiplies $F_L^\gamma(x,Q^2)$ in the differential cross section is very small. Therefore, $F_L^\gamma(x,Q^2)$ cannot be determined from the differential cross-section. Only $F_2^\gamma(x,Q^2)$ can be measured. However, the existence of the longitudinal component can be estimated from the azimuthal correlations of lepton pairs produced via the two-photon interaction (see section 4).

Table 1: Kinematic range of published LEP data.

Expt.	$\sqrt{s}$	Θ_{tag} range	Q^2 range	x range
	GeV	rad.	GeV^2	
ALEPH	91	.060 - .150	6 - 44	.002 - .900
ALEPH	91	$>$ .318	50 - 2400	.000 - .975
DELPHI	91	$>$ .044	3 - 300	.005 - 9.9
DELPHI	183	$>$ .044	10 - 1000	.007 - 0.95
L3	91	.026 - .066	1.2 - 9	.002 - .200
L3	91	.2 - .6	40 - 500	.05 - .98
L3	183	.030 - .066	9 - 30	.01 - .3
OPAL	91	.027 - .055	1.1 - 6.6	.0025 - .2
OPAL	161	.033 - .055	11 - 41	.02 - .6
OPAL	172	.060 - .120	11 - 41	.02 - .6

The kinematic range of the LEP data published up to

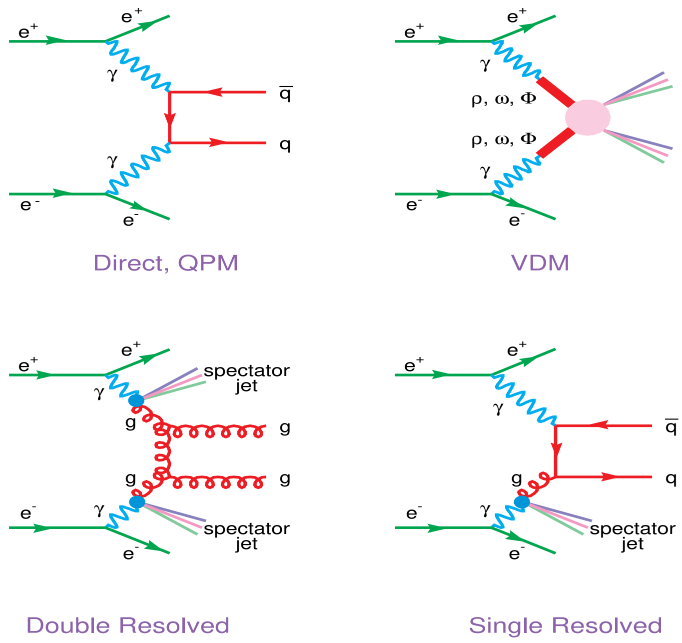

Figure 2: Graphs for the production of hadrons via the two-photon exchange.

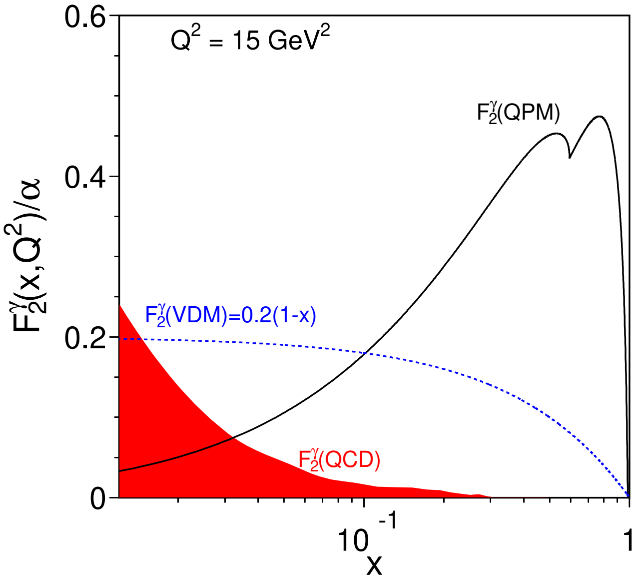

Figure 3: Decomposition of F_2^γ/α into QPM, VDM and QCD at $Q^2 = 15$ GeV^2.

now is displayed in Table 1. Most data have been taken with electron tags in the forward calorimeters. The highest values of Q^2 have been obtained from data where the tagged electrons are measured in the central calorimeters as well. ALEPH (papers # 898a + 898b), L3 (papers # 525 + 1060) and OPAL (papers # 398 + 399) submitted contributions on hadronic structure functions to this conference. On leptonic structure functions, papers were submitted by OPAL (paper # 400) and L3 (paper # 526).

2 Theoretical Expectations

The graphs contributing to the scattering of two virtual photons are displayed in Fig. 2. The main contribution comes from the direct or "QPM" graph which can be seen from Fig. 3 showing the various contributions to F_2^γ/α. as a function of x at $Q^2 = 15$ GeV^2. The small dip in the QPM distribution at x = 0.6 and the less step decrease with decreasing x arises from the $c\bar{c}$ threshold at W = 3 GeV ($x = \frac{15}{15+9}$). The VDM part is rather flat as function of x. QCD contributes via singlet gluons at small x (Monte Carlo estimation in Fig. 3) and via non-singlet gluons to the QPM distribution at large x.

The main questions of interest are:
i) do the data support the rise of the gluonic part of F_2^γ/α at small x which was observed at HERA?
ii) Does the Q^2-evolution agree with the expectations?

3 Hadronic Structure Functions

There are quite a few Monte Carlo programs available for the simulation of the two-photon process. Unfortunately, none of them is completely satisfactory as can be seen below. The PHOJET [1] generator, used by L3, was not specifically developed for the high Q^2 region and contains, hence, only transverse photon cross-sections. In addition, the threshold of $W > 7$ GeV for inclusion of charm quarks is too high. TWOGAM [2] generates the QPM, VDM and QCD processes separately. Both PHOJET and TWOGAM contain a parton transverse momentum cutoff parameter to separate soft from hard processes. PYTHIA [5] and F2GEN [6] have been mainly used by the OPAL experiment. HERWIG [3] was developed for the deep-inelastic two-photon process but does not describe the data well as can be seen from the comparison of the p_t distribution of the L3 data at $\sqrt{s} =$ 91 GeV and $1.2GeV^2 \leq Q^2 \leq 9GeV^2$ (see Fig. 4). Also the pseudo-rapidity distribution of the OPAL data at $< Q^2 > = 13$ GeV shows a deficit of events from the HERWIG generator (Fig. 5).

The M.C. generators are important because the "true" value of x has to be unfolded from the measured value of x with the help of a M.C. simulation. Fig. 6 shows that the visible hadronic mass W_{vis} and the improved mass W_{rec} [a] differ quite substantially from the

[a] Here the kinematics of the tagged electron is included in the calculation of the mass as suggested in Ref. [4].

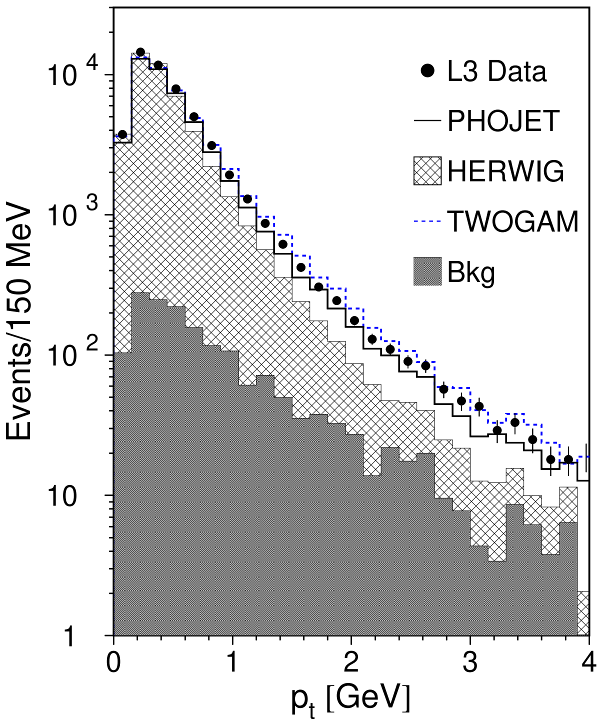

Figure 4: p_t distribution of charged tracks.

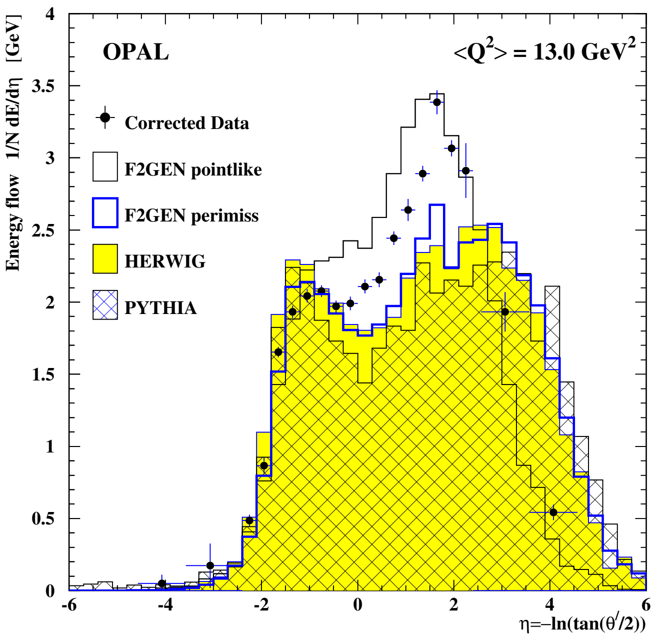

Figure 5: η distributions for $< Q^2 >= 13 GeV^2$ from OPAL:

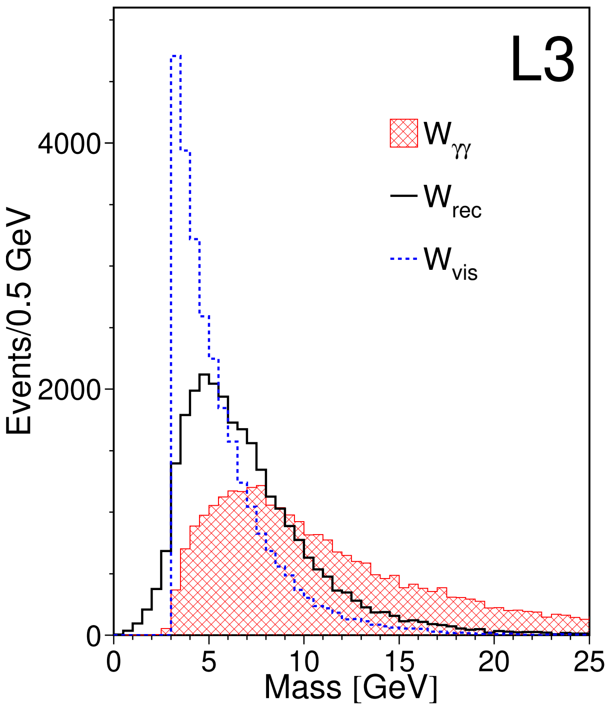

Figure 6: Comparison of W_{vis} and W_{rec} with the true hadronic invariant mass $W_{\gamma\gamma}$.

"true" $W_{\gamma\gamma}$ which enters into the calculation of x. L3 uses the improved variable x_{rec} and the difference of F_2^γ/α obtained after unfolding x_{vis} and once after unfolding x_{rec} is added to the systematic errors.

Fig. 7, finally, shows the measured structure function [b] at low Q^2 from L3 and OPAL and a comparison to four theoretical parameterizations. First, the L3 data and the OPAL data agree very well if the **same** (HERWIG) M.C. generator is used for the unfolding. Second, L3 and OPAL treat the systematic errors differently. L3 shows the structure function unfolded with PHOJET and TWOGAM separately. The statistical and systematic errors are added in quadrature each time. OPAL includes the discrepancy due to the M.C. in the systematic error. The measured values of F_2^γ/α are compared to four theoretical predictions: GRV-L(ow)O(rder)/H(igh)O(order)[7] where the QCD-evolution starts at $Q_0^2 = 0.25 GeV^2$, SaS-1d [8] with $Q_0^2 = 0.36 GeV^2$ and LAC1 [9] where the QCD-evolution starts at a high value of $Q_0^2 = 4 GeV^2$. Comparing the data at low x to the QPM predictions (Fig. 3) one notices the need of gluon contributions since $F_2^\gamma(QPM)/\alpha$ decreases at low x. With some good will one may interpret that the data **and** the parameterizations start to increase with decreasing x. GRV-HO gives

[b] In both cases the data have not been corrected for the non-zero virtuality of the target photon.

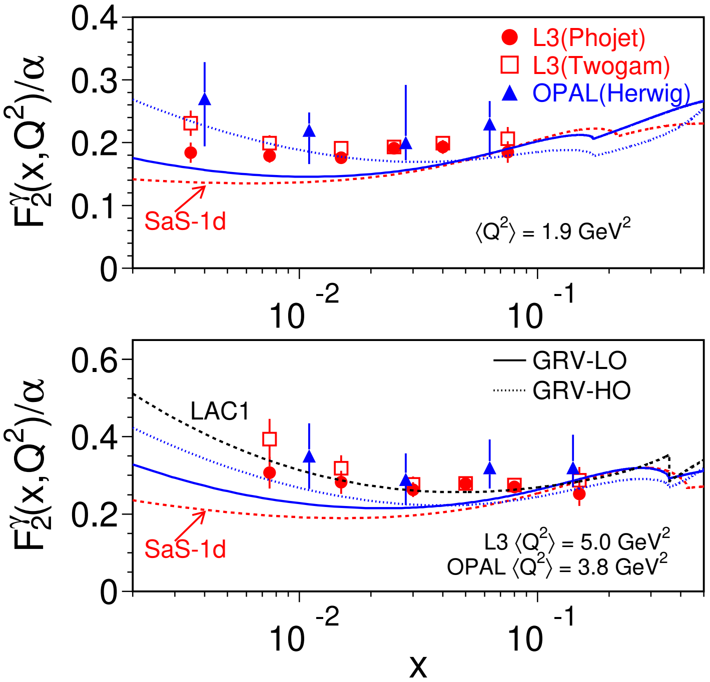

Figure 7: Comparison of the measured F_2^γ/α at $\sqrt{s} = 91$ GeV from L3 and OPAL at low values of Q^2.

the best agreement with the data. It should be noted that in these plots both the M.C. to correct the data and the theoretical calculations have a target virtuality of zero ($P^2 = 0$). In the medium Q^2 bins (see Fig. 8) the rise at small x can no longer be seen since the minimal x values are too high. This plot also shows the improvement in the measurement of F_2^γ/α at LEP with respect to earlier JADE and TASSO measurements.
Finally, for the highest Q^2 data from ALEPH (see Fig. 9) the agreement of F_2^γ/α with the parameterizations is good. It should be noted that the mean value of $< Q^2 > = 279$ GeV^2 covers the region $50 GeV^2 < Q^2 < 2400 GeV^2$.

The same parameterizations are compared to the Q^2-evolution of the data in Fig. 10. LAC1 [c] predicts a too strong increase in the lowest bin of $0.01 < x < 0.1$. Otherwise the Q^2-dependence agrees with the expectations from QCD. In the bin $0.01 < x < 0.1$ the L3 data - when fitted with a form a + b ln Q^2 (solid line in the figure) - yield a somewhat larger slope (b = 0.080 ± 0.013) than expected from GRV-HO (b = 0.061) or SaS-1d (b = 0.043).

[c]According to reference [10] the existing parameterizations do not fulfill the QCD sum rule for leading twist partonic distributions of real and virtual photon targets.

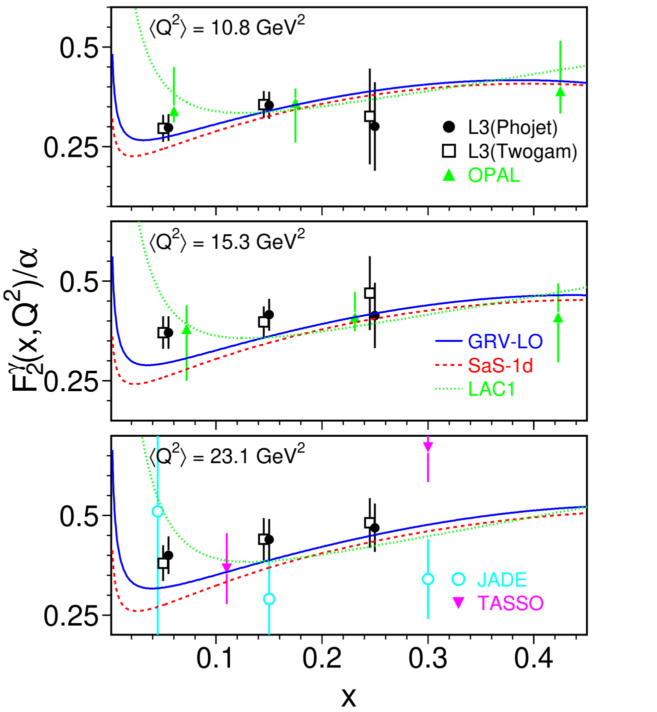

Figure 8: Comparison of the measured F_2^γ/α at LEP2 energies from L3, OPAL, JADE and TASSO at medium values of Q^2.

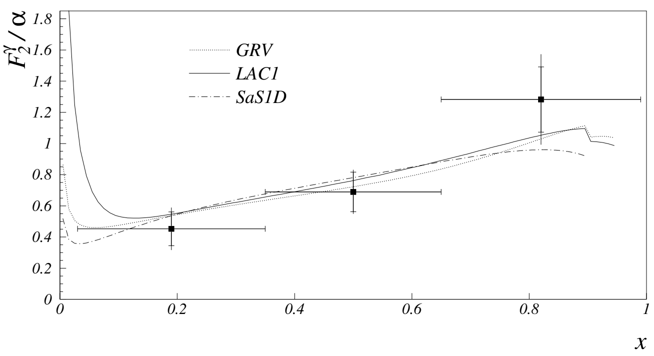

Figure 9: F_2^γ/α from ALEPH at $< Q^2 > = 279$ GeV^2.

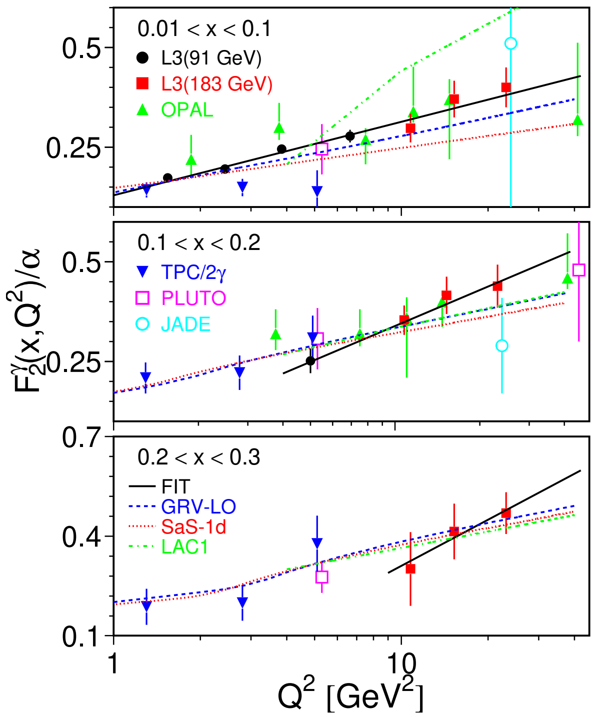

Figure 10: The measured F_2^γ/α from L3 at 91 GeV and 183 GeV, OPAL, ALEPH, TPC/2γ, PLUTO and JADE versus Q^2.

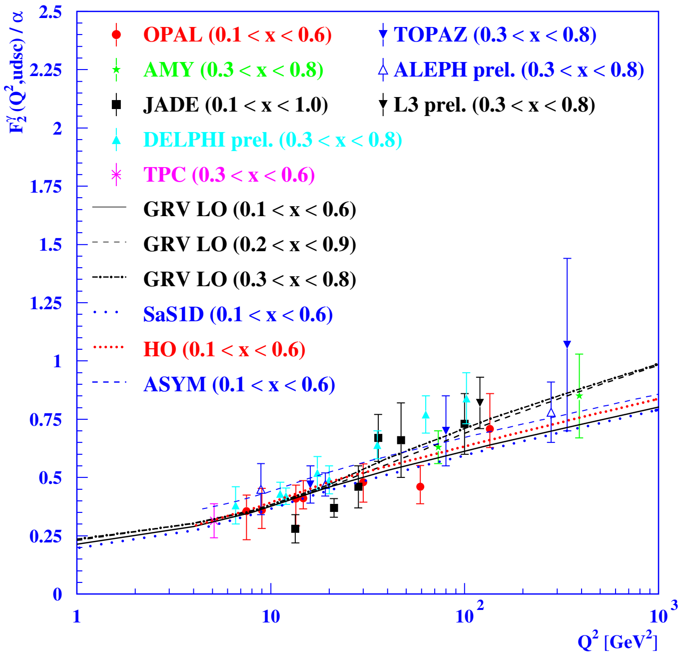

Figure 11: The measured F_2^γ/α from ALEPH, AMY, DELPHI, JADE, L3, OPAL, TOPAZ and TPC versus Q^2.

Finally, Fig. 11 shows a compilation of structure functions from PEP, PETRA and LEP experiments as a function of Q^2. There is no significant deviation of the various parameterization from the scatter of measured values.

4 Leptonic Structure Functions

The interest in the measurement of the leptonic structure function is twofold. On the one hand it allows a test of QED. On the other hand one can check whether longitudinal photon amplitudes exist since the azimuthal correlations of leptons in the $\gamma\gamma$ c.m. system are sensitive to the photon helicity amplitudes. Thus, one can check the existence of F_L^γ which cannot be determined from differential cross-sections as mentioned in section 1. The reaction $e^+e^- \to e^+e^-l^+l^-$ arises from $O(\alpha^4)$ processes Fig. 12 shows the dominant multi-peripheral diagram.

Fig. 13 shows the definition of the polar (Θ^*) and azimuthal angles (χ) of a μ^- in the $\gamma\gamma$ c.m. system. In the single-tag configuration, neglecting the longitudinal component of the target photon, the cross section contains three terms:

$$\frac{d^4\sigma}{dxdydzd\chi} = \frac{2\pi\alpha^2}{Q^2}\frac{1+(1-y)^2}{xy}[A_1(x,z) + A_2(x,z)\cdot\cos\chi + A_3(x)\cdot\cos 2\chi]$$

with $z = cos\Theta^*$. A_1, A_2 and A_3 are related to three differential structure functions $\tilde{F}^\gamma_{T,L,A,B}$:

$$A_1 = \tilde{F}_2^\gamma(x,z) = 2x\tilde{F}_T^\gamma(x,z) + \tilde{F}_L^\gamma(x)$$
$$A_2 = -\tilde{F}_A^\gamma(x,z) \text{ (interference term)}$$
$$A_3 = \tfrac{1}{2}\tilde{F}_B^\gamma(x) \text{ (interference term)}$$

with $F^\gamma_{T,L,A,B} = \int_{-1}^{1}\int_0^{2\pi}\frac{d\chi dz}{2\pi}\tilde{F}^\gamma_{T,L,A,B}$

A_2 describes the interference between a) the amplitude for longitudinal probe photons with transverse target photons and b) the amplitude for transverse probe photons with transverse target photons (see Fig. 14),

This interference term and - after integration - F_A^γ are, hence, proportional to the square-root of the longi-

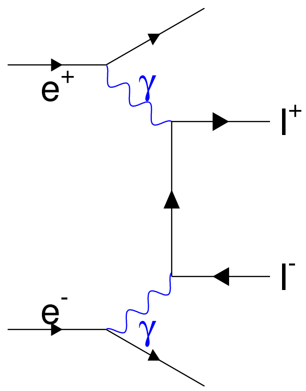

Figure 12: Feynman graph of the reaction $e^+e^- \to e^+e^-l^+l^-$, where l can be any lepton.

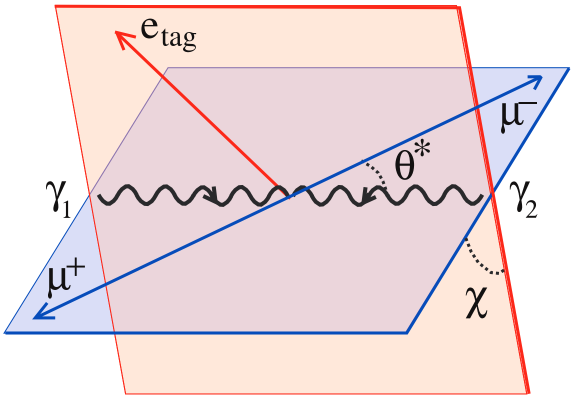

Figure 13: Definition of polar and azimuthal angles of the μ^- in the $\gamma\gamma$ c.m. system.

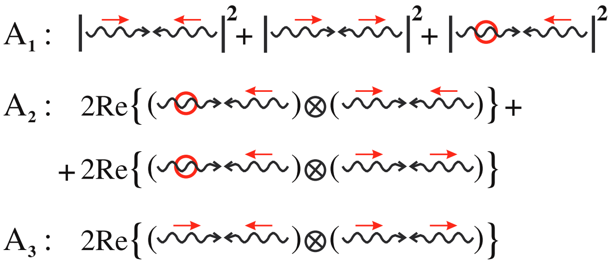

Figure 14: Schematic presentation of the three terms. Probe photons are represented on the left and target photons on the right.

tudinal structure function $\sqrt{F_L^{\gamma}(x,Q^2)}$.

Fig. 15 shows the leptonic structure function F_2^{γ}/α in the range $1.4 GeV^2 \leq Q^2 \leq 7.6 GeV^2$ at $\sqrt{s} = 91$ GeV. The QED prediction with target photon virtuality $P^2 = 0\ GeV^2$ (dashed curve) clearly does not reproduce the data. A fit to QED yields as average $< P^2 >= (0.033 \pm 0.005) GeV^2$ in excellent agreement with the value of $(0.034 \pm 0.002) GeV^2$ calculated [11] including radiative corrections. The data are even sensitive to radiative corrections, since the expected value for P^2 is $(0.024 \pm 0.003) GeV^2$ without radiative corrections, i.e. 1.6 standard deviations lower than the measurement. The target photon virtuality should, therefore, be taken into account when determining structure functions from single-tag data.

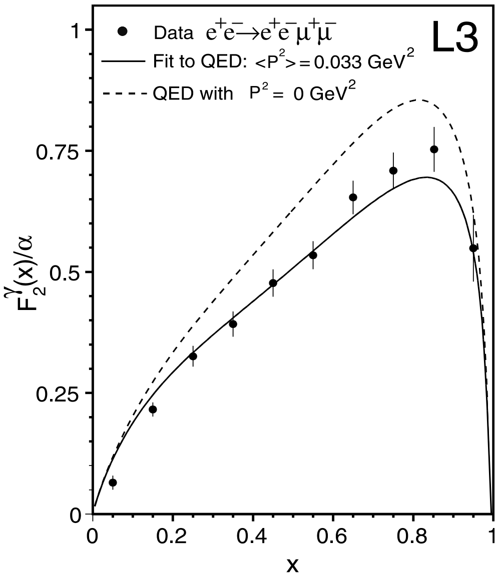

Figure 15: Determination of the leptonic structure function F_2^{γ} in the range $1.4\ GeV^2 \leq Q^2 \leq 7.6\ GeV^2$ (at $\sqrt{s} = 91$ GeV). Only statistical errors are given.

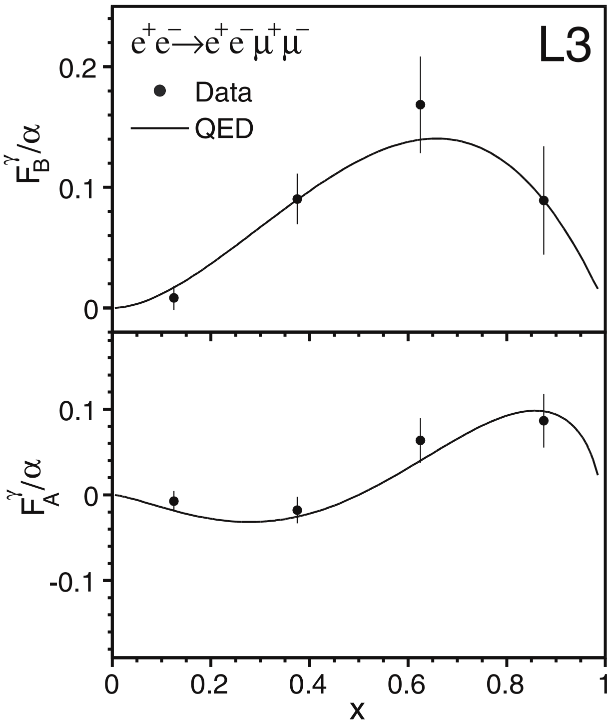

Figure 16: Measurement of the leptonic structure functions F_B^{γ} and F_A^{γ} in the Q^2 range $1.4 GeV^2 < Q^2 < 7.6 GeV^2$ (at $\sqrt{s} = 91$ GeV).

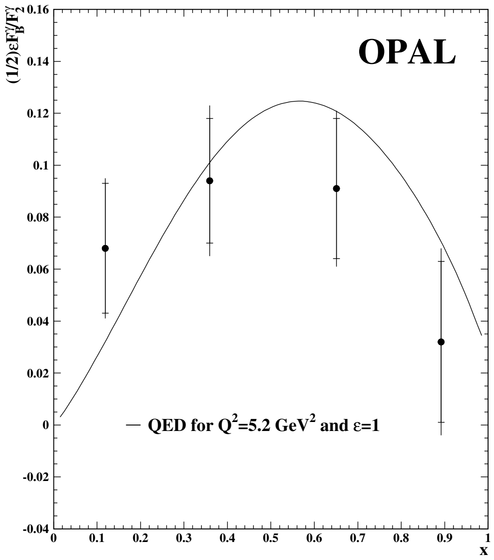

Figure 17: The ration of the leptonic structure functions F_B^γ/F_2^γ from OPAL.

The measured leptonic structure functions F_B^γ and F_A^γ from L3 are displayed in Fig. 16. Fig. 17 shows the ratio of the leptonic structure functions F_B^γ/F_2^γ from OPAL. From both measurements one can conclude: i) F_B^γ and F_A^γ are non-zero. Therefore, F_L^γ(x,Q^2) must be non-zero as well. ii) There is good agreement with QED.

5 Summary

In general, the data on leptonic structure functions reproduce the QED predictions well.

- The virtuality of the target photon is important and should be taken into account also for the determination of the hadronic structure function.
- The data are sensitive to initial state radiation effects.
- The existence of $F_L^\gamma(x, Q^2)$ is established via the interference term in azimuthal angular distributions.

From the measurement of the hadronic structure functions one can conclude:

- At small x (< 0.05) gluon effects are needed to describe the data; the higher order GRV parameterization is preferred for $x < 0.05$.
- The observed Q^2-dependence is compatible with QCD.
- The LAC1 parameterization is ruled out at small x because of a too steep Q^2-dependence. However, it was already ruled out because of a sum rule [10].
- An improvement of the M. C. generators is highly desirable.
- LEP has improved the measurement of the photon structure functions significantly and will do so even more in the future.

Acknowledgements

I would like to thank my colleagues from the L3 two-photon group, in particular F. Erné, J.H. Field, M.N. Kienzle-Focacci and C.H. Lin as well as S. Söldner-Rembold from OPAL for helpful discussions.

References

1. R. Engel, Z. Phys. C 66 (1995) 203;
R. Engel and J. Ranft, Phys. Rev. D 54 (1996) 4244.
2. S. Nova et al., DELPHI Note 90-35 (1990).
3. G. Marchesini et al., Comp. Phys. Comm. 67 (1992) 465.
4. L. Lönnblad et al., "$\gamma\gamma$ event generators", in Physics at LEP2, ed. G. Altarelli, T. Sjöstrand and F. Zwirner, CERN 96-01 (1996), Volume 2, 201.
5. T. Sjöstrand, Comp. Phys. Comm. 82 (1994) 74.
6. A. Buijs et al., Comp. Phys.Comm. 79 (1994) 523; J.J. Ward, PhD Thesis, University College London UCL (1996) unpublished.
7. M. Glück, E. Reya and A. Vogt, Phys. Rev. D 45 (1992) 3986; M. Glück, E. Reya and A. Vogt, Phys. Rev. D 46 (1992) 3986;
8. G.A. Schuler and T. Sjöstrand, Z. Phys. C 68 (1995) 607; G.A. Schuler and T. Sjöstrand, Phys. Lett. B 75 (1996) 193.
9. H. Abramovicz, K. Charchula and A. Levy, Phys. Lett. B 269 (1991) 458.
10. L.L. Frankfurt and E.G. Gurvich, Phys. Lett. B 386 (1996) 379.
11. F.A. Berends, P.H. Daverfeldt and R. Kleiss, Nucl. Phys. B 253 (1985) 421; Comp. Phys. Comm. 40 (1986) 271.